Wideband Polarization Converters Based on Miniaturized-Element Frequency Selective Surfaces

Seyed Mohamad Amin Momeni Hasan Abadi[1] and Nader Behdad[1]

Department of Electrical and Computer Engineering, 1415 Engineering Dr, Madison, WI 53705, USA.

[1]Department of Electrical and Computer Engineering, University of Wisconsin, Madison, Wisconsin, USA.

Abstract. We introduce a new technique for designing wideband polarization converters based on miniaturized-element frequency selective surfaces (MEFSSs). The proposed structure is a two-dimensionally anisotropic periodic structure composed of arrays of sub-wavelength capacitive patches and inductive wire grids separated by thin dielectric substrates. The structure is designed to behave differently for field components of the two orthogonal polarizations and transmits a circularly polarized wave once illuminated by a linearly-polarized plane wave. Using equivalent circuit models for MEFSSs, a synthesis procedure is developed that can be used to design a polarization converter from its required bandwidth of operation. Using this procedure, a prototype of the proposed polarization converter operating within X-band is designed, fabricated, and experimentally characterized using a free-space measurement system. The measurement results confirm the predictions and the design procedure of the structure and demonstrate that the proposed MEFSS-based polarization converter operates in a wide field of view of $\pm 45^{\circ}$.

1. Introduction

Polarization of a wave is an important aspect of its propagation characteristics. In antenna design, the choice of the polarization mostly depends on the application and also the propagation environment. For instance, in satellite communications or navigations systems, circularly-polarized waves are preferred due to the advantages such as lower sensitivity to multipath fading and reduced sensitivity to Faraday rotation or the orientation of the receiver's antenna. In communication systems involving satellite-earth links, a linearly-polarized wave experiences an unpredictable rotation as it propagates through ionosphere. This rotation may cause polarization mismatches at the receiver which consequently reduces the gain of the link budget [*Le Vine et al.*, 2002]. Circularly-polarized waves, on the other hand, do not suffer from these issues and have been used in modern satellite and point-to-point communication systems to improve the polarization efficiency and propagation link budget. Over the past several decades, a variety of different circularly-polarized antenna designs have been reported in the literature. An alternative way of generating a circularly-polarized wave is to generate a linearly-polarized wave and pass it through a polarization converter. This technique is particularly useful where the radiating system consists of a planar array. In such a situation, a polarization converter can be placed on top of the linearly-polarized antenna system to produce circularly-polarized waves.

A polarization converter is a slab of an anisotropic medium that converts an incident wave with a given polarization to a reflected or a transmitted wave with a different polarization (e.g. linear to circular, vertical to horizontal, etc.). Planar polarization converters

are generally implemented using frequency selective surfaces. These structures normally operate based on dividing a wave into two orthogonal components and generating a 90° phase shift between them. A simple implementation for such devices is a reactive surface having inductive impedance for one component of the field and capacitive impedance for the other. This way, a phase shift of 90° appears between the two components of the emerging transmitted wave. In such a situation, if these two components have equal amplitudes, the incident linearly-polarized wave will be converted to a transmitted circularly-polarized wave at the output. Over the past several decades, a number of different types of polarization converters operating in such a fashion have been reported in the literature. The work reported in [*Lerner*, 1965] is among the first structures designed to perform a conversion between linearly-polarized and circularly-polarized waves. This structure is a multilayer structure consisting of both inductive and capacitive impedance sheets. The dimensions of the structure are chosen in such a way to introduce a 90° phase shift between orthogonal field components to achieve a circularly-polarized transmitted wave when the structure is illuminated with a linear-polarized wave. In [*Young et al.*, 1973], a meandered-line polarizer is reported. The converter is a multilayer structure composed of meandered metallic strips. The basic approach in the design of this structure is to make an array that is predominantly inductive to one polarization and capacitive to the orthogonal polarization. This concept was modified and improved in [*Joyal et al.*, 2012; *Letizia et al.*, 2012]. Also, the integration of such converter and a horn antenna was used to design an EBG antenna in [*Letizia et al.*, 2010]. Other than the aforementioned structures, two-dimensional arrays of cross-shaped dipoles [*Kiani et al.*, 2012; *Sohail et al.*, 2013], cross-shaped slots [*Euler et al.*, 2010], split-ring slots [*Euler et al.*, 2010; *Wang et al.*,

2014; *Yan et al.*, 2013], and hexagonal-shaped slots [*Euler et al.*, 2010] with asymmetric features have also been used to design polarization converters. Furthermore, in [*Biscarini et al.*, 2013] and [*Martinez-Lopez et al.*, 2014] multilayer structures composed of arrays of respectively T-shaped slots and bisected split-ring elements were reported. Despite the advantages offered by these structure, most of them use resonant constituting elements and hence, they tend to be narrowband structures. The relatively large dimensions of the resonant constituting unit cells of these structures also deteriorates their performance under oblique incidence angle illumination conditions.

Over the past few years, a new class of metamaterial-inspired frequency selective surfaces with sub-wavelength unit cell dimensions referred to as miniaturized-element frequency selective surfaces (MEFSSs) has been studied [*Behdad et al.*, 2008; *Al-Joumayly et al.*, 2010; *Momeni Hasan Abadi et al.*, 2013]. To date, such structures have been employed in a wide range of devices including spatial filters [*Behdad et al.*, 2008; *Al-Joumayly et al.*, 2010; *Momeni Hasan Abadi et al.*, 2013], transmitarrays [*Al-Joumayly et al.*, 2011; *Li et al.*, 2013; *Momeni Hasan Abadi et al.*, 2014], and reflectarrays [*Edalati et al.*, 2014; *Momeni Hasan Abadi et al.*, 2015]. In this paper, we present a method for designing wideband polarization converters based on MEFSS structures. The proposed converters are composed of two dimensional arrays of capacitive patches and inductive wire grids separated from one another with thin dielectric substrates. Each pixel in the proposed polarization converter is a unit cell of an appropriately-deigned MEFSS with different transmission characteristics for the two orthogonal polarizations. Over the band of interest, the structure is impedance matched for both polarizations while providing two distinct linear phase responses with a phase difference of 90° between the two orthogonal

polarizations. With these principles of operation, the proposed device is capable of offering wideband operation. In addition, due the low profile and the miniaturized element dimensions of the proposed structure, this device can demonstrate a stable performance with a wide field of view. Using this approach, a linear-to-circular polarization converter prototype operating within X-band was designed, fabricated, and experimentally characterized. The measurement results confirm that the fabricated device operates over a bandwidth of more than 40%. The measurements also demonstrate that the structure has a very consistent frequency response as a function of the angle of incidence of the EM wave, with a field of view of $\pm 45^{\circ}$, for both the horizontal and vertical polarizations of incidence.

2. Principles of Operation

Fig. 1 presents the topology of a linear-to-circular polarization converter. This device is a slab of anisotropic medium which converts a linearly-polarized wave to a circularly-polarized one. The device is illuminated with a linearly-polarized incident wave with the electric field vector, $\vec{E}^i$, tilted 45° relative to both $\hat{x}$ and $\hat{y}$ directions. $\vec{E}_x^i$ and $\vec{E}_y^i$ are the vertical and horizontal components of the incident electric field, respectively. This polarization converter behaves differently for these two components. Specifically, the device has two distinctive frequency responses for the vertical and horizontal components of the incident wave. Within the operational band, the magnitude of the transmission coefficient for both components is ideally equal to one and the device passes both components very efficiently within the pass band with little attenuation. However, vertical and horizontal components experience two distinct phase shifts with the phase difference of 90° while propagating through the converter. As a result, within the transmission window, the po-

larization of the emerging wave at the other side will be circular. $\vec{E}_x^t$ and $\vec{E}_y^t$ are the two orthogonal components of the transmitted wave and are expressed in terms of $\vec{E}_x^i$ and $\vec{E}_y^i$ using the following formulas:

$$\vec{E}_x^t = T_x \vec{E}_x^i \tag{1}$$

$$\vec{E}_y^t = T_y \vec{E}_y^i \tag{2}$$

where $T_x = |T_x| e^{j\measuredangle T_x}$ and $T_y = |T_y| e^{j\measuredangle T_y}$ are the transmission coefficients of the device for the $\hat{x}$ and $\hat{y}$ polarizations, respectively. To achieve a circularly-polarized wave at the output within the operational band, T_x and T_y are related based on the following formulas:

$$|T_x| = |T_y| \tag{3}$$

$$\measuredangle T_y - \measuredangle T_x = \pm \frac{\pi}{2} \tag{4}$$

The sign in (4) determines the sense of rotation of the circularly-polarized output wave. The transmitted wave is as right-handed circularly polarized if $\measuredangle T_y - \measuredangle T_x = \frac{\pi}{2}$ and left-hand circularly-polarized if $\measuredangle T_y - \measuredangle T_x = -\frac{\pi}{2}$.

The polarization converter shown in Fig. 1 is implemented using miniaturized-element frequency selective surfaces. The elements of the MEFSS structures including capacitive patches and wire grids are often rotationally symmetric and hence, polarization independent (for normal incidence angle). Polarization converters, on the other hand, need to have different responses for $\hat{x}$- and $\hat{y}$-polarized waves. Therefore, the present structure needs to feature asymmetric elements within a unit cell to generate two distinct frequency responses for vertical and horizontal components of the incident wave. Fig. 2 shows the

three-dimensional topology of the proposed polarization converter. The structure consist of two-dimensional periodic arrangement of sub-wavelength capacitive patches and planar wire grids, separated from one another by thin dielectric substrates. Assuming that thickness of the substrate between two consecutive metallic layers is h, the overall thickness of the structure is $(N-1)\times h$, where N is the total number of metallic layers used to implement the structure. The top view of one unit cell of the capacitive layer and that of an inductive layer are shown in the inset of Fig. 2. The dimensions of the unit cell along the $\hat{x}$ and $\hat{y}$ directions are $D_x = D_y = D$. The capacitive patches are in the form of rectangular metallic patches with dimensions of $D - s_x^i$ and $D - s_y^i$, where s_x^i and s_x^i are the gap spacings between two adjacent patches in i^{th} layer in $\hat{x}$ and $\hat{y}$ directions, respectively. The inductive wire grids are the combination of two metallic strips with the widths of w_x^i and w_y^i oriented perpendicularly to each other. Due to these asymmetric features, this structure will have different responses for incident plane waves polarized in the $\hat{x}$ and $\hat{y}$ directions.

The synthesis procedure of MEFSSs are typically based on a generalized equivalent circuit model, whose values are determined from the system level performance indicators such as the center frequency of operation, operational bandwidth, response type, etc. In the proposed device, the structure of the equivalent circuit model is the same for both polarizations with the exception of the element values as shown in Fig. 3. In this circuit model, the capacitive patches are modeled with parallel capacitors $C_x^1, C_x^3.., C_x^N$ for $\hat{x}$ polarization, while these capacitors are $C_y^1, C_y^3.., C_y^N$ for $\hat{y}$ polarization. The inductive wire grids are represented by parallel inductors $L_x^2, .., L_x^{N-1}$ and $L_y^2, .., L_y^{N-1}$ for the $\hat{x}$ and $\hat{y}$ polarizations, respectively. Thin substrates separating the inductive and the ca-

pacitive layers are modeled with transmission lines with the characteristic impedances of $Z_{1,2}, ..., Z_{N-1,N}$ and the lengths of $h_{1,2}, ..., h_{N-1,N}$ for both polarizations. For non-magnetic media $Z_{i,i+1} = Z_0(\varepsilon_r^{i,i+1})^{-1/2}$. Free space on each side of the device is modeled with semi-infinite transmission lines with characteristics impedance of $Z_0 = 377\ \Omega$.

As described in [*Li et al.*, 2013; *Momeni Hasan Abadi et al.*, 2014], MEFSSs can be used as time delay units. To act as time-delay units, they must be designed to provide linear phase responses with desired slopes versus frequency over a wide range of frequencies in their transmission windows (i.e. to provide desired, constant group delays). Therefore, if the proposed structure is designed to exhibit a linear phase response for both $\hat{x}$ and $\hat{y}$ polarizations while maintaining a phase difference of 90° between the two responses, a wideband polarization converter can be achieved. This concept is depicted in Fig. 4. In this figure, T_x and T_y are the transmission coefficients of the converter for $\hat{x}$ and $\hat{y}$ polarizations, respectively. The transmission windows for $\hat{x}$- and $\hat{y}$ polarizations are respectively $\Delta f_t^x = f_H^x - f_L^x$ and $\Delta f_t^y = f_H^y - f_L^y$. The overlap frequency band between the two responses is shown as $\Delta f_d = f_H^x - f_L^y$. The operational band of interest for the converter is also denoted as $\Delta f_{opt} = f_H - f_L \leq \Delta f_d$. The total phase span within the transmission windows is $\Delta\phi_t$ for both polarizations as this parameter is only a function of the order of the response of the MEFSS used to construct the device ($\frac{N+1}{2}$ where N is the number of metallic layers). The relation between these two parameters can be expressed as $\Delta\phi_t = \frac{(N+1)\pi}{4}$. For an ideal case, the frequency response for the $\hat{x}$ polarization is a de-tuned version of the frequency response for the $\hat{y}$ polarization while ensuring that the desired phase and amplitude responses are maintained. Therefore, the bandwidth of both responses and their total phase shifts within their transmission

windows are $\Delta f_t = \Delta f_t^x = \Delta f_t^y$ and $\Delta\phi_t$, respectively. In that case, to achieve an operational bandwidth of Δf_{opt}, the transmission window for each of the two responses can be calculated using the following formula:

$$\Delta f_t \geqslant \frac{\Delta f_{opt}}{\left(1 - \frac{\Delta\phi_d}{\Delta\phi_t}\right)} \tag{5}$$

where $\Delta\phi_d$ is the desired phase difference of 90° in an ideal situation. For example, if the total phase span of the transmission coefficient for both polarizations is 270°, then, the bandwidth of the each response needs be at least 1.5 times the desired bandwidth of the converter $\Delta f_t = 3/2 \times \Delta f_{opt}$. As described, the total phase shift provided by an MEFSS is a function of the order of the response. Therefore, for a design with higher number of layers, a narrower transmission window for each polarization is required.

3. Design Procedure

The design procedure of the proposed polarization converter is based on synthesizing the transmission characteristics of the required responses for both vertical and horizontal polarizations. These responses are determined based on the operational band of interest $\Delta f_{opt} = f_H - f_L$. To do so, the structure is first designed based on the equivalent circuit model and then the physical and geometrical parameters (e.g. wire widths and gap spacings) are calculated using Eqs. (23)-(24) in [*Al-Joumayly et al.*, 2010]. The design procedure of the proposed device consists of a few different steps. This design starts by determining the order of the response of the MEFSS ($\frac{N+1}{2}$) for both polarizations (i.e. number of metallic layers N). This parameter can be chosen arbitrarily as long as the total phase shift is more than 90°. A high number of order may result in complexity of the design. The resulting high-profile structure also may suffer from deterioration of response

under oblique incidences. A low number of order, on the other hand, my cause difficulties to achieve all the goals over the band of interest. Knowing the order of the response, $\frac{N+1}{2}$, and Δf_{opt}, the minimum operational bandwidth for responses for the $\hat{x}$ and $\hat{y}$ polarizations (i.e. Δf_t^x and Δf_t^y) can be determined using Eq. (5). After determining the order of the response and the bandwidth for each polarization, the values of the elements of the circuit models shown in Fig. 3 can be calculated using the procedure described in Section II of [*Al-Joumayly et al.*, 2010]. However, to ensure that the phase difference between the two components remains 90° over the band of interest, a modified procedure needs to be followed. In this procedure, the initial values of the elements of the equivalent circuit model for both polarizations are determined based on the synthesis procedure described in [*Al-Joumayly et al.*, 2010]. Then, one of the initial responses is kept the same and the other one is tuned to achieve the design goals. The tuning is performed by optimizing the parallel inductor and capacitor values. The specific design goals for this optimization step are to have a have a transmission window overlap and a phase difference of 90° over the entire operational band of interest. Alternatively, this goal can be considered as achieving a required axial ratio for the transmitted signal within the frequency band of operation. This parameter can be determined using the following formula:

$$AR = \left(\frac{|T_x|^2 + |T_y|^2 + \sqrt{a}}{|T_x|^2 + |T_y|^2 - \sqrt{a}} \right) \tag{6}$$
$$a = |T_x|^4 + |T_y|^4 + 2|T_x|^2|T_y|^2 \cos\left(2(\measuredangle T_y - \measuredangle T_x)\right)$$

Assuming that T_y is synthesized first and T_x is then determined in the de-tuning step, the optimization parameters are the values of the parallel capacitors $C_x^1, ..., C_x^N$ and those of the parallel inductors $L_x^2, ..., L_x^{N-1}$ in the equivalent circuit model shown in Fig. 3. The thicknesses of the substrates are already determined while T_y is synthesized. To

accomplish the optimization step, two method can be envisioned. First, it can be done using a circuit simulation software (e.g. Agilent Advance Design System®). Alternatively, the transfer function of an MEFSS can also be predicted using its equivalent circuit model:

$$T = \frac{2}{A + \frac{B}{Z_0} + CZ_0 + D} \tag{7}$$

where A, B, C, and D are given by:

$$\begin{bmatrix} A & B \\ C & D \end{bmatrix} = \left(\prod_{i=1,\, i\, odd}^{N-2} \mathbf{T}_C^i \mathbf{T}_h^{i,i+1} \mathbf{T}_L^{i+1} \mathbf{T}_h^{i+1,i+2} \right) \mathbf{T}_C^N \tag{8}$$

In Eq. (7), $\mathbf{T}_C^i$, $\mathbf{T}_L^i$, and $\mathbf{T}_h^{i,i+1}$ can be calculated using the following formulas:

$$\mathbf{T}_C^i = \begin{bmatrix} 1 & 0 \\ j\omega C_x^i & 1 \end{bmatrix} \tag{9}$$

$$\mathbf{T}_L^i = \begin{bmatrix} 1 & 0 \\ (j\omega L_x^i)^{-1} & 1 \end{bmatrix} \tag{10}$$

$$\mathbf{T}_h^{i,i+1} = \begin{bmatrix} \cos\beta h_{i,i+1} & jZ_{i,i+1}\sin\beta h_{i,i+1} \\ (j/Z_{i,i+1})\sin\beta h_{i,i+1} & \cos\beta h_{i,i+1} \end{bmatrix} \tag{11}$$

where $Z_{i,i+1}$ and $\beta = \frac{\omega\sqrt{\varepsilon_r^{i,i+1}}}{c}$ are respectively the characteristic impedance and propagation constant of the transmission lines. Combination of (7)-(11) yields a relationship between the phase and magnitude of the frequency response (i.e. $\angle T_x$ and $|T_x|$) and the element values in the equivalent circuit model shown in Fig. 3. Using these equations is an alternative method for performing the optimization. In the final step, after calculating all the element values of the equivalent-circuit models shown in Fig. 3, the geometrical parameters including the strip widths and gap spacings can be determined using equations (23)-(24) of [*Al-Joumayly et al.*, 2010].

4. A Design Example, Experimental Verification, and Measurement Results

The procedure presented in Section 3 was followed to design a polarization convertor operating at the entire X-band covering the frequency range of 8 GHz to 12 GHz or equivalently a 40% fractional bandwidth. A third-order bandpass MEFSS was used to design this polarization converter. With this order of response, the total phase shift over the entire main transmission window is 270°. Based on Eq. (5), this phase shift requires a minimum bandwidth of 6 GHz for each of the horizontal and vertical responses. Following the design procedure, to meet the minimum bandwidth requirement and having $f_L^y \leq f_L$, a frequency response with center frequency of 12 GHz and the bandwidth between 7.75 GHz to 16.25 GHz for the $\hat{y}$ polarization was synthesized using the design procedure presented in [*Al-Joumayly et al.*, 2010]. In doing so, first the element values of the equivalent circuit model of the structure including the values of three capacitors, two inductors, and the thicknesses of the dielectric substrates were determined. In this design, the dielectric substrates were assumed to be non-magnetic and have a dielectric constant of ϵ_r=10.2 (Rogers RT/duroid 6010). These circuit values are reported in Table 1. The frequency response for the horizontal ($\hat{x}$) polarization was also synthesized similar to the procedure used for the vertical ($\hat{y}$) polarization. To do so, a frequency response with a center frequency of 8 GHz and the bandwidth between 3.75 GHz and 12.25 GHz was considered. The circuit values to achieve such a response are listed in Table 1. Fig. 5 shows the transmission coefficient for both polarizations as well as the difference between their transmission phases using the circuit values reported in Table 1. The structure for both polarizations is assumed to be symmetric with respect to the center capacitive layer. Thus, in the next step, the element values of the equivalent circuit model for the horizontal

($\hat{x}$) polarization including $C_1^x = C_5^x$, C_3^x, and $L_2^x = L_4^x$ were de-tuned to achieve the design goals. As described in Section 3, this step can be accomplished using optimization in ADS or simply using Eqs. (7)-(11) to numerically perform the optimization. The final element values of the equivalent circuit model for both the horizontal and the vertical polarizations are listed in Table 2. Fig. 6(a) shows the frequency responses predicted using the circuit models with the values reported in Table 2. The difference between the transmission phases of responses for the horizontal and the vertical polarizations predicted using circuit models is also shown in Fig 6(b).

The unit cell dimension of the designed structure is selected to be 4.5 mm, which is equivalent to approximately $0.15\lambda_0$, where λ_0 is the free-space wavelength at the center frequency of operation $f_c = 10$ GHz. Therefore, using $D = 4.5$ mm and the capacitance and inductance values reported in Table 2, the widths of inductive wire grids and capacitive gap spacings can be calculated. Since the proposed structure is a multilayer structure, the effect of the bonding layers placed between the adjacent substrates on its response should also be considered. The bonding materials used in this design is Rogers 4450F prepreg with the dielectric constant of $\epsilon_r = 3.52$ and the thickness of $h_b = 0.1$ mm. Introduction of the bonding layers creates an asymmetry in the topology of the structure, which can slightly change the frequency response of the device. This asymmetry can be eliminated by using two closely spaced patches on the two sides of the middle bonding layer as shown in Fig. 7 instead of using just one patch placed on only one side of this layer. The final physical parameters of the structure are listed in Tabel 3. The structure was simulated in CST Microwave Studio®and its frequency response for both the horizontal and the vertical polarizations was calculated. Fig. 6(a) shows the full-wave simulated transmission

coefficients of the polarization converter for both polarization alongside the frequency responses predicted by the equivalent circuit model. The phase difference between the transmission phases of both polarizations is also shown in Fig. 6(b). Using Eq. (6), the axial ratio of the transmitted signal was also calculated based on the two responses. Fig. 8 shows the predicted axial ratio of the transmitted wave based on both the full-wave simulated results and those obtained using the equivalent circuit model. Observe that the full-wave simulated results are consistent with the predictions from the equivalent circuit model. The axial ratio remains below 1.4 ($\approx$ 3dB) between 7.92 GHz to 12.54 GHz, which successfully covers the entire X-band.

A prototype of the proposed polarization converter was fabricated using standard PCB lithography and substrate bonding techniques. The fabricated prototype has six metallic layers and four dielectric substrates. The panel dimensions of the fabricated prototype are 33.75 cm $\times$ 22.5 cm ($\approx 11.25\lambda_0 \times 7.5\lambda_0$). The total thickness of the structure, including the bonding layers, is 5.4 mm which is approximately equivalent to $0.18\lambda_0$ at 10 GHz. The photograph of the fabricated prototype is shown in Fig. 9. The fabricated prototype was characterized using free-space measurement techniques. To so, the frequency response of the prototype was measured using the technique presented in Section IV of [*Momeni Hasan Abadi et al.*, 2013] and the axial ratio was calculated in the post processing using Eq. (6). The measured frequency responses for both the horizontal and the vertical polarizations, the difference between the phase shifts of both responses, and the axial ratio of the transmitted signal for a normally-incident wave all along with the simulation results obtained using both equivalent circuit model and the full-wave EM simulations are

shown in Figs. 6(a), 6(b), and 6(c), respectively. Observe that a good agreement between the measured and simulated results is achieved.

The sensitivity of the response of the fabricated prototype to the angle of incidence was also examined for various angles of incidence in the range of 0° to 45°. The simulated and measured results for the axial ratio of the transmitted signal for oblique incidences in the range of $0° - 45°$ in both $x - z$ and $y - z$ planes of incidence are shown in Fig. 10(a)-(d). Observe that the structure demonstrates a relatively stable operation over the entire band of interest for incident angles in the range of $\pm 45°$.

5. Conclusions

A new technique for designing low-profile linear-to-circular polarization converters with wide bandwidths was presented. The proposed structure is a multilayer structure composed of reactive impedance surfaces separated from one another by thin dielectric substrates. Providing different transmission characteristics for the two orthogonal polarizations, the proposed device is able to convert a linearly-polarized wave with an electric field rotated 45° relative to these orthogonal polarizations to a circularly-polarized wave. In doing so, this device is impedance matched for both polarization while introducing a 90° difference between the transmission phases of the two orthogonal components of the incident wave within the frequency band of interest. A design procedure was also presented and used to a design a prototype capable of operating over the entire X-band in the 8-12 GHz frequency range. A prototype of the device was also fabricated and experimentally characterized using a free-space measurement setup. The measurements confirmed the consistent performance of the converter within over 40% bandwidth. The performance of this structure for oblique angles of incidence was also experimentally characterized. It

was observed that the structure provides a stable frequency response for oblique incidence angles in the $\pm 45^{\circ}$ range in both $x-z$ and $y-z$ planes of incidence.

Acknowledgments. This material is based upon work supported by the National Science Foundation under NSF award ECCS-1101146.

References

D. M. Le Vine and S. Abraham (2002), The effect of the ionosphere on remote sensing of sea surface salinity from space: absorption and emission at L band, *IEEE Trans. on Geoscience and Remote Sensing*, vol. 40, no. 4, 771-782.

D. Lerner (1965), A wave polarization converter for circular polarization, *IEEE Trans. Antennas Propag.*, vol. 13, no. 1, pp. 3-7.

L. Young, L. A. Robinson, and C. A. Hacking, Meander-line polarizer (1973), *IEEE Trans. Antennas Propag.*, vol. 21, no. 3, pp. 376-378.

M. Joyal and J. Laurin (2012), Analysis and design of thin circular polarizers based on meander lines, *IEEE Trans. Antennas Propag.*, vol. 60, no. 6, pp. 3007-3011.

M. Letizia, B. Fuchs, C. Zorraquino, J. F. Zurcher, and J. R. Mosig (2012), Oblique incidence design of meander-line polarizers for dielectric lens antennas, *Prog. Electromagn. Res. B*, vol. 45, pp. 309-335.

E. Arnaud , R. Chantalat , M. Koubeissi , T. Monediere , E. Rodes, and M. Thevenot (2010), Global design of an EBG antenna and meander-line polarizer for circular polarization, *IEEE Antennas Wireless Propag. Lett.*, vol. 9, pp. 215-218.

G. Kiani, V. Dyadyuk, "Low loss FSS polarizer for 70 GHz applications (2012)," *Ant. And Propagat. Soc. Int. Symp. (APSURSI)*, pp. 1-2.

I. Sohail, Y. Ranga, K. Esselle, and S. Hay (2013), A linear to circular polarization converter based on jerusalem-cross frequency selective surface, *7th. Eur. Conf. Antennas Propag. (EuCAP2013)*, pp. 2141-2143.

M. Euler, V. Fusco, R. Cahill, and, R. Dickie (2010), Comparison of frequency-selective screen-based linear to circular split-ring polarisation convertors, *Microw. Antennas Propag.*, vol. 4, no. 11, pp. 1764-1772.

M. Euler, V. Fusco, R. Cahill, and R. Dickie (2010), 325 GHz single layer sub-millimeter wave FSS based split slot ring linear to circular polarization convertor, *IEEE Trans. Antennas Propag.*, vol. 58, no. 7, pp. 2457-2459.

J. Wang, W. Wu, and Z. Shen (2014), Improved polarization converter using symmetrical semi-ring slots, *Ant. And Propagat. Soc. Int. Symp. (APSURSI)*, pp. 1-2.

S. Yan and G. A. E. Vandenbosch (2013), Compact circular polarizer based on chiral twisted double split-ring resonator, *Appl. Phys. Lett.*, vol. 102, no. 10, pp. 103503.

M. Biscarini, G. M. Sardi, E. Maritini, F. Caminita, and S. Maci (2013), A simple croad-band FSS polarizer, *7th. Eur. Conf. Antennas Propag. (EuCAP2013)*.

L. Martinez-Lopez, J. Rodriguez-Cuevas, J. I. Martinez-Lopez, and A. E. Martynyuk (2014), A multilayer circular polarizer based on bisected split-ring frequency selective surfaces, *IEEE Antennas Wireless Propag. Lett.*, vol. 13, pp. 153-156.

N. Behdad, A second-order band-pass frequency selective surface using non-resonant sub-wavelength periodic structures (2008), *Microw. Opt. Technol. Lett.*, vol. 50, no. 6, pp. 1639-1643.

M. Al-Joumayly and N. Behdad (2010), A generalized method for synthesizing low-profile, band-pass frequency selective surfaces with nonresonant constituting elements, *IEEE*

Trans. Antennas Propag., vol. 58, no. 12, pp. 4033-4041.

S. M. A. Momeni Hasan Abadi, M. Li, and N. Behdad (2014), Harmonic-suppressed miniaturized-element frequency selective surfaces with higher order bandpass responses, *IEEE Trans. Antennas Propag.*, vol. 62, no. 5, pp. 2562-2571.

M. Al-Joumayly and N. Behdad (2011), Wideband planar microwave lenses using sub-wavelength spatial phase shifters, *IEEE Trans. Antennas Propag.*, vol. 59, no. 12, pp. 4542-4552.

M. Li, M. Al-Joumayly, and N. Behdad (2013), Broadband true-time-delay microwave lenses based on miniaturized element frequency selective surfaces, *IEEE Trans. Antennas Propag.*, vol. 61, no. 3, pp. 1166-1179.

M. Li and N. Behdad, Wideband true-time-delay microwave lenses based on metallo-dielectric and all-dielectric lowpass frequency selective surfaces, *IEEE Trans. Antennas Propag.*, vol. 61, no. 8, pp. 4109-4119.

S. M. A. Momeni Hasan Abadi and N. Behdad (2014), Design of wideband, FSS-based multibeam antennas using the effective medium approach, *IEEE Trans. Antennas Propag.*, vol. 62, no. 11, pp. 5557-5564.

A. Edalati and K. Sarabandi (2014), Reflectarray antenna based on grounded loop-wire miniaturised-element frequency selective surfaces, *IET. Microw. Antennas Propag.*, vol. 8, no. 12, pp. 973-979.

S. M. A. Momeni Hasan Abadi, K. Ghaemi, and N. Behdad (2015), Ultra-wideband, true-time-delay reflectarray antennas using ground-plane-backed, miniaturized-element frequency selective surfaces, *IEEE Trans. Antennas Propag.*, vol. 63, no. 2, pp .534-542.

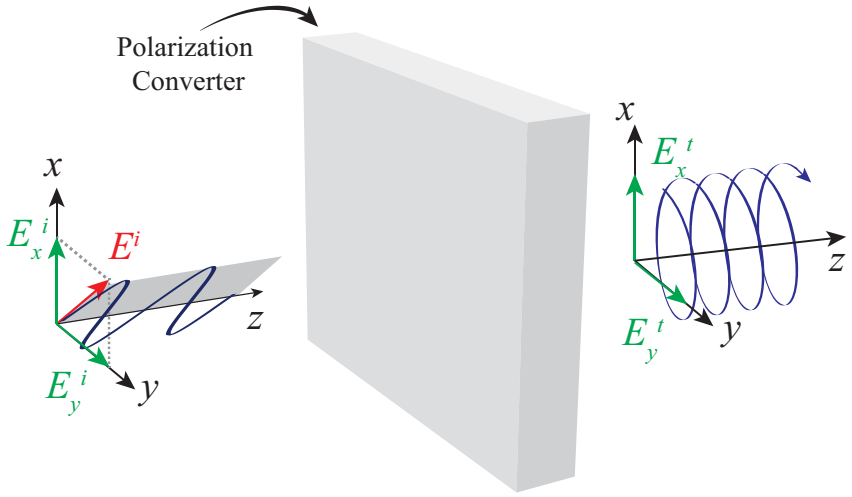

Figure 1. Schematic model of a linear-to-circular polarization converter. In this configuration, the incident electric field vector is tilted 45° relative to $\hat{x}$ and $\hat{y}$ directions. After passing through the converter, the transmitted signal is right-handed circularly polarized.

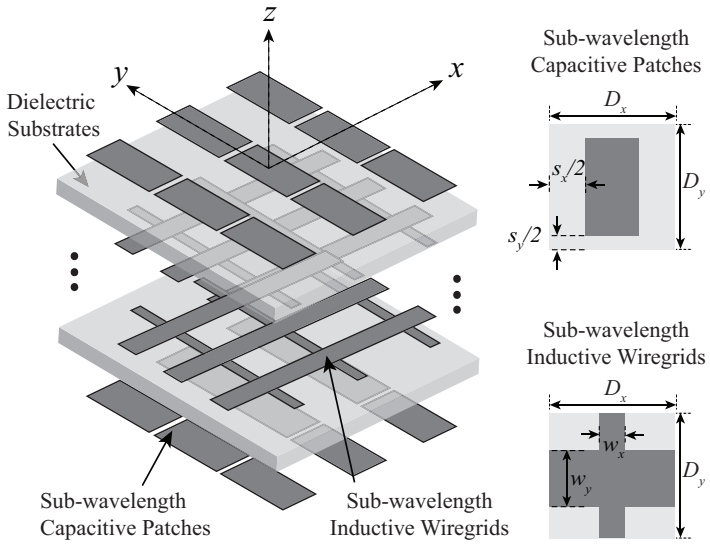

Figure 2. Topology of the proposed polarization converter based on bandpass miniaturized-element frequency selective surfaces. The unit cells of the capacitive patches and the inductive wire grids are shown on the right hand side of the figure.

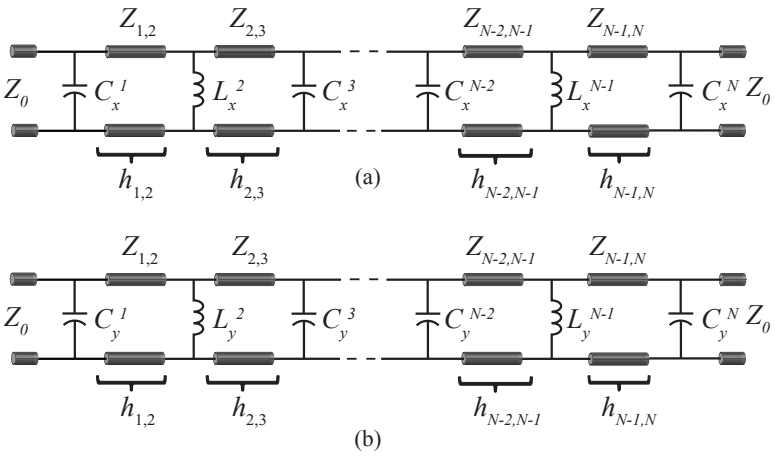

Figure 3. Equivalent circuit model of the converter shown in Fig. 2 for (a) the horizontal ($\hat{x}$-directed) and (b) the vertical ($\hat{y}$-directed) polarizations.

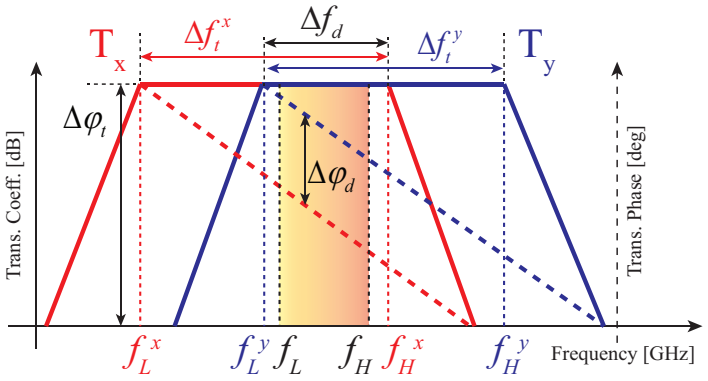

Figure 4. The concept of de-tuning to design a wideband polarization converter. T_x and T_x shows the frequency response of the device for horizontal ($\hat{x}$) and vertical ($\hat{y}$) polarizations, respectively. The transmission windows for $\hat{x}$ and $\hat{y}$ polarizations are respectively $\Delta f_t^x = f_H^x - f_L^x$ and $\Delta f_t^y = f_H^y - f_L^y$. In this configuration, Δf_d is the overlapping region between the two responses and Δf_{opt} shows the operational band of interest in which the structure is impedance matched for both orthogonal polarizations while there is a 90° phase difference between their corresponding transmission phases.

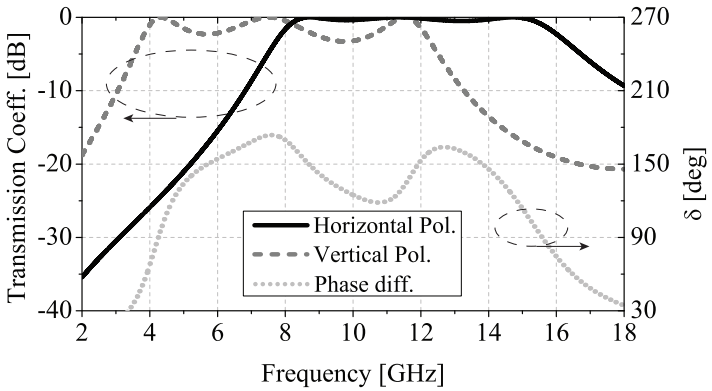

Figure 5. Calculated transmission coefficients of the polarization converter discussed in Section 4 as well as the difference between the corresponding transmission phases with the parameters shown in Table 1.

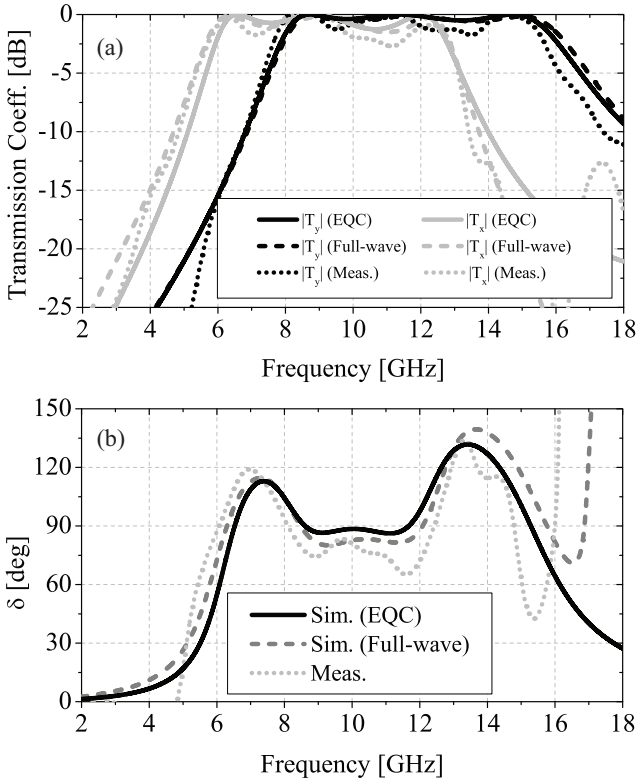

Figure 6. Simulated and measured transmission characteristics of the polarization converter discussed in Section 4. These characteristics include (a) transmission coefficients for the two orthogonal polarization and (b) the difference between their corresponding transmission phases.

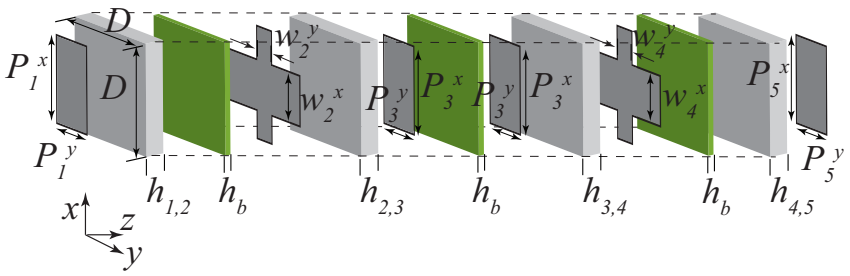

Figure 7. Unit cell of the proposed polarization converter discussed in Section 4. Notice that the two capacitive patches placed in the center are separated from one another by a thin prepreg layer. These two layers consititute a single hybrid capacitive layer. This arrangement is used to maintain the symmetry of the structure as discussed in Section 4.

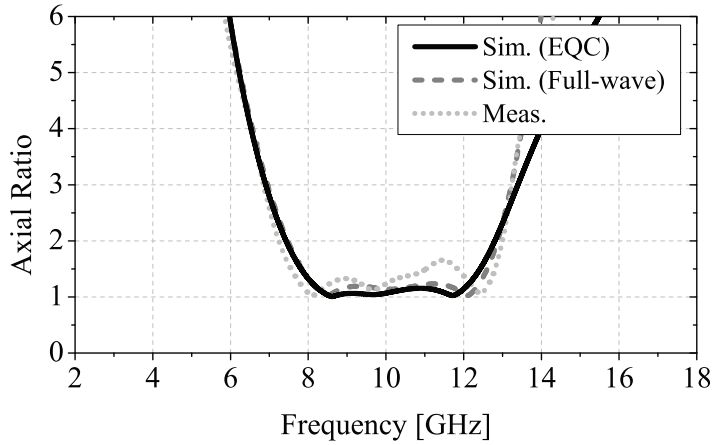

Figure 8. Simulated and measured axial ratios of the polarization converter discussed in Section 3. These results are obtained using Eq. (6) with the values obtained from the simulated and measured magnitude and phase of the response of the FSS for both $\hat{x}$ and $\hat{y}$ polarizations.

Table 1. The element values of circuit models shown in Fig. 3 to have third-order responses with $\Delta f_x = 3.75$ GHz-12.25 GHz and $\Delta f_y = 7.75$ GHz - 16.25 GHz for the horizontal and vertical polarizations, respectively.

Parameter	$C_1^y = C_5^y$	C_3^y	$L_2^y = L_4^y$	$L_2^x = L_4^x$
value	23 fF	46 fF	1.1 nH	3.5 nH
Parameter	$C_1^x = C_5^x$	C_3^x	$h_{1,2} = h_{4,5}$	$h_{2,3} = h_{3,4}$
value	90 fF	120 fF	1.27 mm	1.27 mm

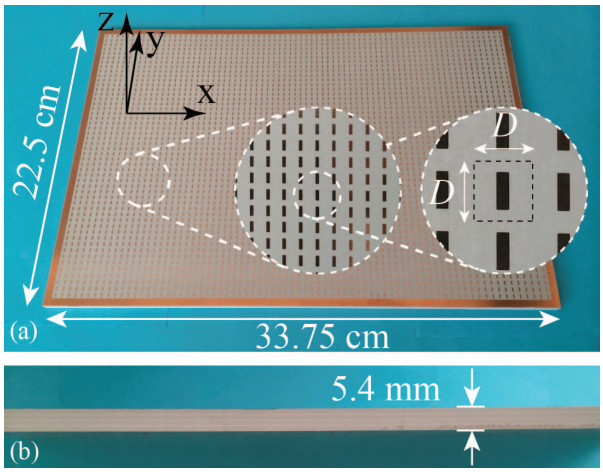

Figure 9. (a) Photograph of the fabricated polarization converter. (b) Side view of the fabricated prototype.

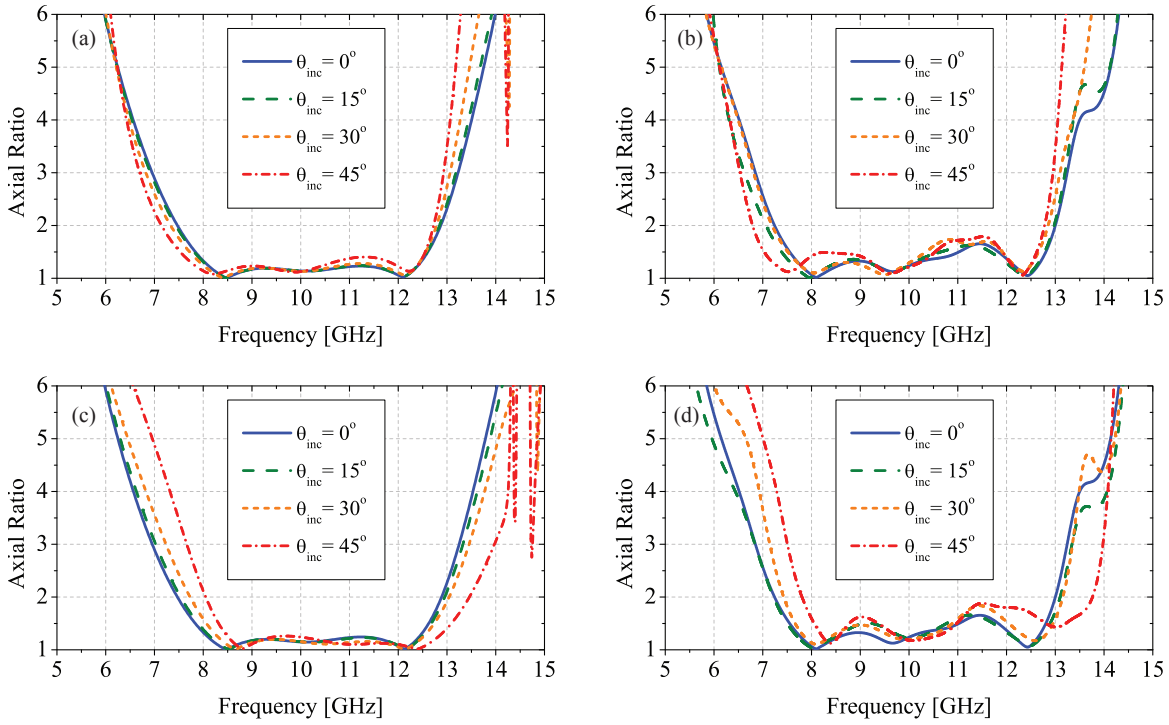

Figure 10. (a),(c) Simulated and (b),(d) measured axial ratios of the transmitted wave passed through the polarization converter for an incident wave propagating in (a),(b) $x-z$ and (c),(d) $y-z$ planes of incidence.

Table 2. The finalized element values of the equivalent circuit models shown in Fig. 3 for the polarization converter discussed in Section 4.

Parameter	$C_1^y = C_5^y$	C_3^y	$L_2^y = L_4^y$	$L_2^x = L_4^x$
value	23 fF	46 fF	1.1 nH	1.49 nH
Parameter	$C_1^x = C_5^x$	C_3^x	$h_{1,2} = h_{4,5}$	$h_{2,3} = h_{3,4}$
value	67 fF	112 fF	1.27 mm	1.27 mm

Table 3. Physical parameters of the polarization converter discussed in 4, with the unit cell shown in Fig. 7 and with the equivalent circuit model element values reported in Table 2. The unit cell dimension for this structure is $D = 4.5mm$.

Parameter	$P_1^y = P_5^y$	P_3^y	$w_2^x = w_4^x$	$w_2^y = w_4^y$
value	1 mm	1.6 mm	0.8 mm	0.2 mm
Parameter	$P_1^x = P_5^x$	P_3^x	$h_{1,2} = h_{4,5}$	$h_{2,3} = h_{3,4}$
value	2.9 mm	2.5 mm	1.27 mm	1.27 mm

College of Engineering
UNIVERSITY OF WISCONSIN-MADISON

March 8, 2015

To whom it may concern:

I am writing this letter to confirm that my contribution to the paper titled "Wideband Polarization Converters Based on Miniaturized-Element Frequency Selective Surfaces," by S. M. A. Momeni Hasan Abadi and N. Behdad is advisory and the main contribution is that of Mr. Seyed Mohamad Amin Momeni Hasan Abadi. Therefore Amin is eligible to participate in the student paper competition of the 2015 North American Radio Science Meeting. If you have any questions about this letter or need any additional information, please feel free to contact me via phone or email.

Sincerely,

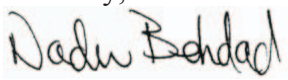

Nader Behdad, Ph.D.
Associate Professor in Electrical and Computer Engineering

Department of Electrical and Computer Engineering, University of Wisconsin-Madison
1415 Engineering Drive, Madison, WI 53706 USA
Tel: 608-262-8804 Fax: 608-262-1267 E-mail: behdad@wisc.edu